Tailoring MoS_2 Valley-Polarized Photoluminescence with Super Chiral Near-Field

Ziwei Li[1,2], Changxu Liu[3], Xin Rong[1], Yang Luo[1], Liheng Zheng[1,2], Yongji Gong[4], Shuang Zhang[3], Zheyu Fang[1,2]**

[1]School of Physics, State Key Lab for Mesoscopic Physics; Collaborative Innovation Center of Quantum Matter, Peking University, Beijing 100871, China

[2]Academy for Advanced Interdisciplinary Studies, Peking University, Beijing 100871, China

[3]School of Physics and Astronomy, University of Birmingham, Birmingham, B15 2TT, UK

[4]School of Materials Science and Engineering, Beihang University, Beijing 100191, China

Transition metal dichalcogenides (TMDs) with intrinsic spin-valley degrees of freedom hold great potential in the applications of spintronic and valleytronic devices. Monolayer MoS_2 possesses two inequivalent valleys in Brillouin zone, and each valley couples polarized photons with specific helicity in the regime of quantum mechanism. Degree of valley polarization (DVP) is a parameter to characterize the purity of valley-polarized photoluminescence (PL) of monolayer MoS_2. Usually, the detected value of DVP in monolayer MoS_2 shows achiral property with opposite helicities excitation due to reciprocal phonon-assisted intervalley scattering process. Here, we report that valley-polarized PL of MoS_2 can be tailored with near-field interaction of plasmonic chiral metasurface. The resonance of chiral metasurface generates particular chiral near-field, couples with valley-polarized excitons, and tailors the PL spectra detected in far-field. Due to the tailoring effect, chiral DVP of monolayer MoS_2 has been observed with opposite helicities excitation, and furthermore, valley-contrast PL can be pumped by linear polarized light in our chiral heterostructure. The manipulation of valley-polarized PL in two-dimensional materials presents a solid step towards the optically accessible route for valley-polaritonic devices.

KEYWORDS: *valley-polarized PL, degree of valley polarization, chirality, exciton-plasmon interaction, MoS_2*

Introduction

The spin and valley degrees of freedom in semiconductor are potential choices for exploiting new condensed-matter phenomena, which have been studied for a plethora of applications in spintronic devices and valley-selective light-emitters.[1-3] The manipulation of valley degree of freedom remains a large unexplored area, and it may open up the way of exploiting the intriguing spin-valley physics for future quantum technology. An excellent valleytronic material should have a band structure composed of two (or more) degenerate but inequivalent valley "states", which are usually related with spin electrons (holes) occupation near the band extrema.[4, 5] In the field of spin-electronic devices, manipulation of the spin electrons provides a feasible method to realize valley-dependent carriers transport.[6] However, the ability to control valley-polarized photoluminescence (PL) has been rather limited, which needs the selective addressing of distinct valleys through an external control, and also acquires that the valleys are direct band gap with high PL efficiency.

The research of valley-polarized photoluminescence has been burgeoning with the rapid development of two-dimensional (2D) honey-combed structure, such as graphene, 2D transition metal dichalcogenides (TMDs).[7-9] TMDs are van der Waals layered-semiconductors with direct band-gap energy in the visible spectral range.[10, 11] Benefiting from the properties of broken inversion symmetry and strong spin-orbit coupling of electrons, TMDs possess two inequivalent valleys K and K' in Brillouin zone. These valleys (K and K') show distinct responses to light with opposite helicities, in other words, right (RCP) and left-handed circularly polarized (LCP) photons couple to interband transitions in the K and K' valley, respectively.[8] Monolayer MoS_2 is a member of TMDs family, and valley selectivity properties of pure MoS_2 have been studied among valley selective rules[9], inter-valley scattering[12], exciton valley-Hall effect[13] and valley-dependent opto-electronic devices[14, 15]. Recently, strong-coupling of

exciton-polariton has been reported in monolayer MoS_2 inserted micro-cavities, which helps to develop unique half-light half-matter system towards engineering valley-polaritonic devices.[16-18] TMDs interacting with nanowires and metasurfaces show direction-selective exciton-polariton propagation, which is arising from the effect of angular momentum coupling in hybrid system.[19] However, tailoring the exciton emission of specific valley has less been studied, which may help to develop the advanced circularly polarized light-emitting devices.

Light coupled to plasmonic nanostructures can induce coherent oscillations of surface electrons, which leads to enhanced electromagnetic response in the near-field.[20] It has been reported that chiral plasmonic nanostructures show circular dichroism spectra,[21-23] which enhances the optical activity with chemical molecules and DNA structures.[24-26] This kind of enhancement is named as optical chirality *C*, which is sensitively related with environmental electromagnetic fields.[27-29] High enhancement and large continuous regions of the optical chirality are important factors for tailoring the chirality of light-matter interactions. Benefiting the advantages of chiral nanostructure and microcavity, a hybrid structure may show chiral near-field distribution and field-enhanced light-matter interactions, which can be applied to control the polarization state of exciton radiation.[30-33]

In this article, we utilise metal-dielectric-metal plasmonic chiral structures to investigate the manipulation of valley-polarized PL in MoS_2-metasurface heterostructure. CVD-grown monolayer MoS_2 was sandwiched in a micro-cavity formed by plasmonic chiral metasurface and golden reflection layer. The DVP in monolayer MoS_2 was observed as 25±2% at 87 K due to intervalley scattering. Compared to pure MoS_2, the DVP in MoS_2-metasurface was increased to 43±2% under the excitation of LCP light (σ-), while it decreased to 20±2% under the excitation of RCP light (σ+). The distributions of electromagnetic field and optical chirality provide strong evidences for this near-field tailoring effect. We observe a chiral DVP with opposite helicities excitation in MoS_2-metasurface heterostructure, and moreover, valley polarization phenomenon has been realized under the excitation of linear

polarized laser. The capability to enhance valley-polarized PL distinctly shows a great opportunity towards the future development in valley-dependent optoelectronic devices.

Results

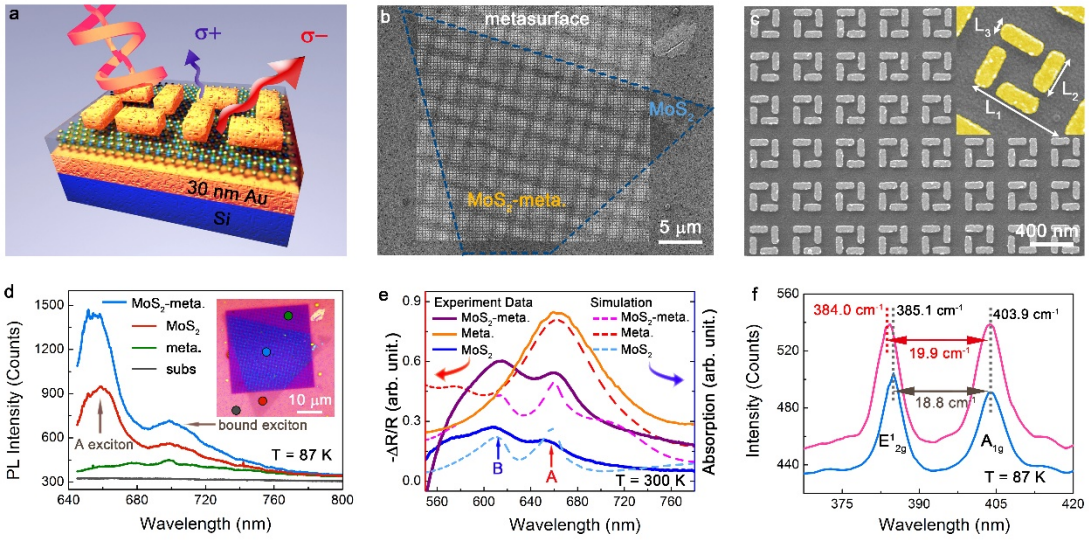

Figure 1 | Structure and spectral properties of MoS_2-metasurface heterostructure. (a) Schematic of MoS_2-metasurface structure, where CVD-grown monolayer MoS_2 is placed into the SiO_2 layer, and sandwiched between chiral metasurface and golden film. Valley-polarized PL of MoS_2 are tailored with near-field interaction under the excitation of specific circular polarized light. (b) The SEM image of MoS_2-metasurface structure fabricated by e-beam lithography, scale bar is 5 μm. (c) SEM image of MoS_2-metasurface with the unit cell of 400×400 nm (scale bar is 400 nm). Inset is the SEM image of metasurface unit. L1, L2 and L3 are the unit length 400 nm, rod length 190 nm and rod width 75 nm. (d) PL spectra of sample obtained from different regions as the positions shown in the inset optical image, scale bar is 10 μm. (e) The experiments (solid lines) and simulations (dashed lines) of spectral absorption obtained from pure MoS_2, metasurface and MoS_2-metasurface. (f) Raman spectra of MoS_2 and MoS_2-metasurface structure. Frequency differences of E^1_{2g} and A_{1g} between MoS_2 and MoS_2-metasurface are 18.8 cm^{-1} and 19.9 cm^{-1}, respectively.

MoS_2-metasurface structure and spectral properties. Figure 1a shows the schematic of the MoS_2-metasurface heterostructure with C4 symmetric nanorods under the excitation of circularly polarized light. The monolayer MoS_2 interacts with the near-field modes resulting in great enhancement of specific valley-polarized PL. The MoS_2-metasurface heterostructure was fabricated in a series of micro-nano processing steps, and the substrate consists of 30 nm metasurface/25 nm SiO_2/30 nm Au/Si. MoS_2 monolayers were sandwiched in SiO_2 dielectric layer, and also placed between

metasurface and golden reflection layer. Figure 1b presents the SEM image of MoS_2-metasurface structure with the scale bar of 5 μm. From the gray contrast of SEM image, CVD-grown MoS_2 monolayer can be distinctly observed as the dashed line shown. The MoS_2 film was grown in a shape of triangle due to its 2H crystal phase, and the length of a side is about 40 μm. The metasurface shows greater brightness in the SEM image due to its metallic properties. Figure 1c shows the SEM image of MoS_2-metasurface with the scale bar of 400 nm. Inset shows the SEM image of metasurface unit with high magnification. L1 (400 nm), L2 (190 nm) and L3 (75 nm) are the statistical average values of period length, rod length and rod width (See Supplementary S2).

Figure 1d shows the PL spectra of the sample at 87 K, which were measured from several positions as shown in the inset optical image. Two characteristic PL peaks of MoS_2 monolayer are observed from the spectral measurements, one is the main direct band-gap transition (A exciton, 660 nm), and the other is the defect-state transition (bound exciton, 700 nm). The PL intensity of MoS_2-metasurface is enhanced compared with pure MoS_2 under the excitation of linear-polarized 633 nm laser, which is arising from the near-field electromagnetic modes induced emission enhancement. The PL intensity of metasurface structure is weak, and the PL energy is away from the A exciton energy but covers the energy of bound exciton. There is no PL signals obtained from the substrate, which excludes the influence of remaining PMMA in a wetting transfer process. More detailed PL spectra of MoS_2 and MoS_2-metasurface are shown in Fig. S1 (See Supplementary S1). Figure 1e shows the absorption spectra of pure MoS_2, metasurface and MoS_2-metasurface in experiments (solid lines) and simulations (dashed lines) at room temperature of 300 K. The main absorption peak of metasurface is around 665 nm with a wide spectral shape. The intrinsic absorption peaks of MoS_2 monolayer is direct band-gap A (654 nm) and B exciton (609 nm). The energy difference (140 meV) of A and B exciton is arising from the spin-orbit coupling of electrons in valence band. With the near-field interaction of exciton and metasurface, both the characteristic absorption peaks A and B are increased obviously. And their

peaks redshift to 660 nm (A exciton) and 615 nm (B exciton), which is due to the coupling of exciton and plasmon. The absorption spectra simulated by COMSOL consist well with the experiment results. More detailed absorption and reflection spectra of metasurface obtained from experiments and simulations are presented in Supporting Information. (See Supplementary S3). The monolayer property of MoS_2 film can be verified by the frequency difference of in-plane (E^1_{2g}) and out-of-plane (A_{1g}) as shown in Fig. 1f. The frequency differences of phonon modes obtained from MoS_2-metasurface (pink line) and MoS_2 film (blue line) are 19.9 cm^{-1} and 18.8 cm^{-1}, respectively. And Raman signals are dramatically enhanced on MoS_2-metasurface structure, which is arising from the surface plasmon enhanced Raman scattering.[33] The shift of E^1_{2g} mode (1.1 cm^{-1}) that induced by the strong electron-phonon coupling provides strong evidence of near-field interaction effect.[34]

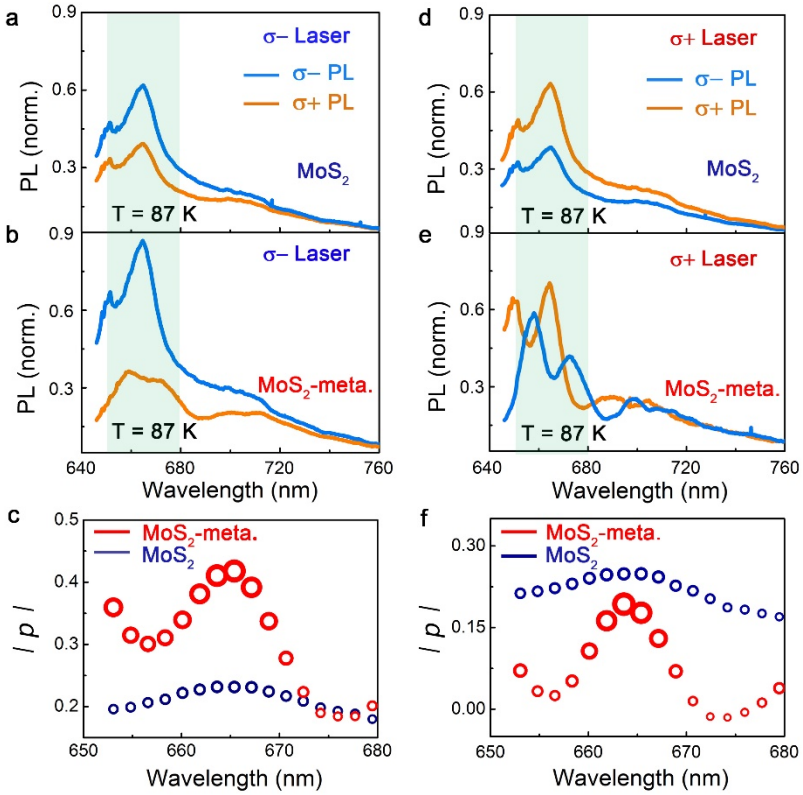

Figure 2 | Valley-polarized PL spectra of MoS_2 and MoS_2-metasurface. (a-b) Circularly polarized PL spectra of MoS_2 and MoS_2-metasurface under the excitation of σ- light (633 nm) at 87 K. (d-e) Circularly polarized PL spectra of MoS_2 and MoS_2-metasurface under the excitation of σ+ light (633 nm) at 87 K. The DVP of MoS_2 and MoS_2-metasurface under σ- excitation (c) and σ+ excitation (f).

Valley-polarized PL. With the near-field interaction of MoS_2 and metasurface, the valley polarization phenomenon was explored using polarized excitation and circularly polarized PL measurements. Figure 2 shows the polarized PL detection of monolayer MoS_2 and MoS_2-metasurface under the excitation of LCP light. The excitation laser is a 633 nm He-Ne laser, which energy (E_{pump} = 1.96 eV) is close to the A exciton energy (E_A = 1.88 eV). Linear polarizer (633 nm) and quarter-wave plate (633 nm) were placed after the laser irradiation to obtain circularly polarized excitation. And a pair of broadband linear polarizer and quarter-wave plate (400-800 nm) were placed before the spectrometer system. All the polarized PL measurements are operated at the temperature of 87 K in a liquid nitrogen–assisted cooling stage.

From the valley-dependent optical selection rule of TMDs, the K' valley can only couples and absorbs the LCP light with spin angular momentum (σ- = -1), and store the σ- exciton in the K' valley. However, optical phonon assisted valley scattering participates in this unsteady process. Some excitons may scatter and occupy in the neighboring K valley with angular momentum exchange(??) (σ+ exciton). The intervalley scattering effect leads to impure detection of polarized PL, which mixes both LCP and RCP light as shown in Fig. 2a. In Figure 2b, the intensity of σ- PL is intensively boosted due to the enhancement of electromagnetic near-field. The intensity of σ+ PL is decreased and the spectral shape changes, which are due to the interactions of σ+ exciton and chiral near-field modes. The DVP p has widely been used to analyze the purity of polarized PL, and it is expressed as $p = (I_- - I_+) / (I_- + I_+)$ in our work. I_+ and I_- are the RCP and LCP PL intensity obtained from the experiments, respectively. Figure 2c shows the DVP of pure MoS_2 and MoS_2-metasurface. A degree of 25±2% has been obtained from monolayer MoS_2, which consists with previous reports ranging from 20% to 35%.[35] Notably, the DVP of MoS_2-metasurface rises up to 43±2% at the A exciton energy ranging from 650 to 680 nm.

Under the excitation of RCP light, the polarized PL spectra and DVP are also plotted in Fig. 2d-e. The polarized PL spectra of monolayer MoS_2 shows the similar results with LCP excitation in Fig.2d, which is fully expected under the mechanism of valley-

dependent optical selection rule. In Figure 2e, the intensities of σ+ and σ- PL detected from MoS_2-metasurface are at the same level, but spectral shapes are different. It fluctuates with the wavelength, arising from the field interference between localized resonance of the metasurface and SPP resonance on golden film. The absolute value of DVP of monolayer MoS_2 shows the same results under different polarized excitation as shown in Fig. 2c and Fig. 2f, owing to the reciprocal intervalley scattering process. The DVP of MoS_2-metasurface with σ+ excitation is suppressed to 20±2% at the energy of A exciton in Fig. 2f. The similar results of valley-polarized PL were observed in Sample 2 with inverse chirality of metasurface (See Supplementary S4).

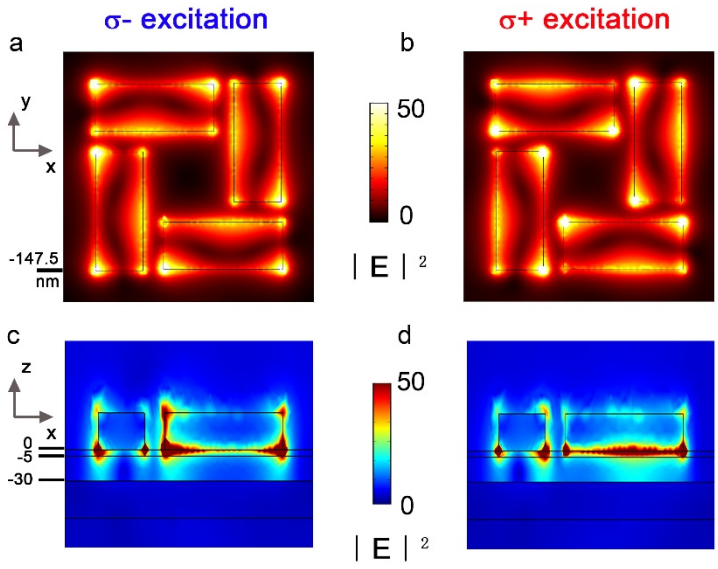

Figure 3 | Electromagnetic field distribution at 633 nm. (a-b) Electromagnetic field distribution under σ- and σ+ excitation at the plane z = -5 nm. (c-d) Near-field electromagnetic field distribution under σ- and σ+ excitation at the plane y = -147.5 nm.

Discussions on super chiral near-field. The far-field valley-polarized PL spectra are resulted from the near-field interaction of valley exciton and surface plasmon modes. The mechanism of near-field interaction can be analyzed with the simulations of electromagnetic field modes by COMSOL. Figure 3a-b show the distributions of electromagnetic field under σ- and σ+ excitation at the plane z = -5 nm, which is the locating layer of monolayer MoS_2. The difference of near-field modes excited from opposite circularly polarized light can be observed clearly. The hot-spots of electromagnetic field mainly locate at the corners and along the edge of nanorods,

which is similar with the distribution of photonic local density of states (LDOS, See Supplementary S5). The electromagnetic field at the out contour corners of metasurface shows the largest intensity with σ- excitation, while at the inner contour corners with σ+ excitation.

Figure 3c-d show the cross-section view of electromagnetic field distribution under σ- and σ+ excitation at the plane y = -147.5 nm. The difference in field distribution can be distinguished clearly, and most of the field energy permeates into the dielectric layer and couples with monolayer MoS_2. The maximum of field enhancement is obtained as large as 50, which is arising from the tiny gaps between nanorods and also between metasurface and golden film. The field distributions with σ- and σ+ excitation are different, however, the far-field reflection spectra are almost the same in two cases (See Supplementary S5). It is suggested that the valley-polarized PL manipulation may not arise from the far-field optical absorption, but from the near-field coupling of exciton-plasmon in the absorption and emission process.

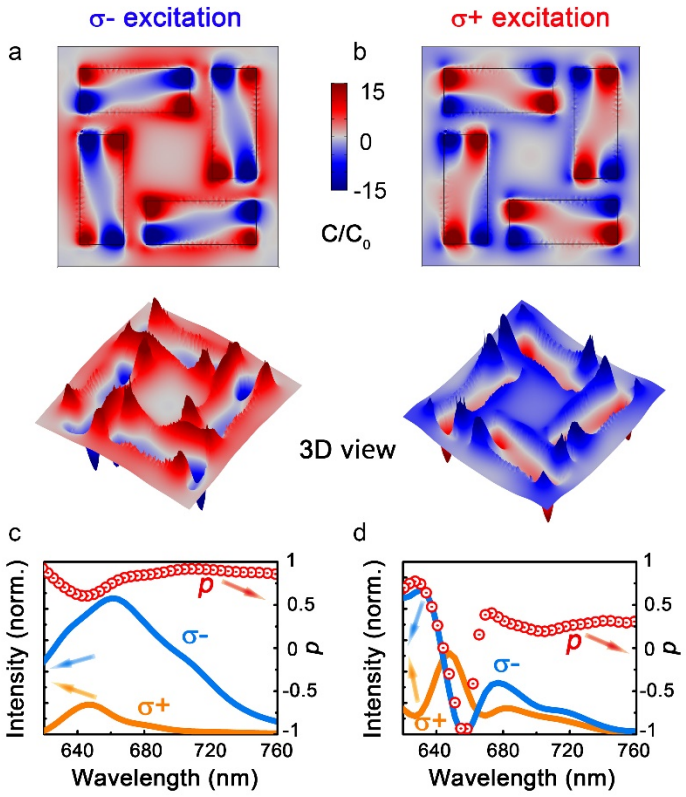

Figure 4 | Super chiral field at 665 nm. (a-b) Near-field optical chirality distributions under σ- and σ+ excitation at the plane z = -5 nm, and their 3D view. (c-d) Simulation of far-field PL spectra and DVP.

The near-field optical chirality distributions are simulated at the resonant absorption of metasurface at 665 nm, as shown in Fig. 4a-b. As reported, some chiral metasurface can significantly enhance the signals detected from chemical and biological molecules. This kind of enhancement are named as optical chirality C,[28] which is a time-even pseudoscalar to analysis the near-field chirality, and it can be obtained as

$$C(\vec{r}) = \frac{1}{2}\left[\varepsilon_0 \vec{E}(\vec{r}) \cdot \vec{\nabla} \times \vec{E}(\vec{r}) + \frac{1}{\mu_0} \vec{B}(\vec{r}) \cdot \vec{\nabla} \times \vec{B}(\vec{r}) \right]$$

where $\vec{E}$ and $\vec{B}$ are the electric and magnetic fields, respectively, and ε_0 and μ_0 are permittivity and permeability of vacuum. A simple version of C can be deduced as

$$C(\vec{r}) = -\frac{\varepsilon_0 \omega}{2} \mathrm{Im}\left[\vec{E}^*(\vec{r}) \cdot \vec{B}\ (\vec{r}) \right]$$

The optical chirality C has been analyzed in different excitation situations. When chiral metasurface interacts with σ- excitation, most of chiral fields surrounded the nanostructures show positive C/C_0 as large as 15. C_0 is the value of optical chirality obtained for circularly polarized light without the metasurface. The enhancement C/C_0 is larger than most of the planar nanostructures reported, which can be named as super chiral field. However, chiral field shows opposite sign of C with σ+ excitation as shown in Fig. 4b. Observed from the 3D view of chiral field, the fields are inhomogeneous as observed inside and outside of nanostructures, and the dominant phenomena of valley polarized PL arise from the contribution of exciton neighboring the border of nanostructures. Exciton inner the nanostructures is covered and contributes less to PL detection.

Here we suggest the exciton of monolayer MoS_2 is purely dipolar excitation, and the dipole excitation of MoS_2 is closely related with C with the inherent valley-dependent chiral properties, as explained as

$$A_{\pm} \propto \alpha \omega E_{\pm} - \beta C_{\pm}$$

where ω and E are the angular frequency and the local electric energy density of the surrounding field, respectively. α is the imaginary part of the electric polarizability, while β is the imaginary part of the mixed electric-magnetic polarizability. The symbol ± represents the excitation of RCP (+) and LCP (-) light. The difference in $A^{\pm}$ therefore

closely depends on the optical chirality *C* induced by nanostructures. A quantum theory model has also been discussed to give a more general explanation (See Supplementary S7).

Besides, the exciton emission process is related with the chiral metasurface. In the FDTD simulation, 100 pairs of left-handed and right-handed electrical dipoles are placed randomly overlapping the period of metasurface, the far-field monitor has been detected to distinguish the left-handed (σ-) and right-handed (σ+) polarized field intensity as shown in Fig. 4c-d (See Supplementary S8). In the simulation of left-handed polarized dipoles, σ- intensity is dramatically enhanced compared with σ+ intensity. The DVP is larger than 75% near the resonant wavelength 665 nm. However, when it happens with right-handed polarized dipoles, σ- intensity is lower than σ+ intensity near the resonant wavelength 665 nm. The DVP shows obvious fluctuation with the wavelength, which consists well with the experimental results in Fig. 2. It is demonstrated that valley-polarized PL manipulation is arising from the near-field coupling effect in two processes, including enhanced exciton absorption and coupled optical emission.

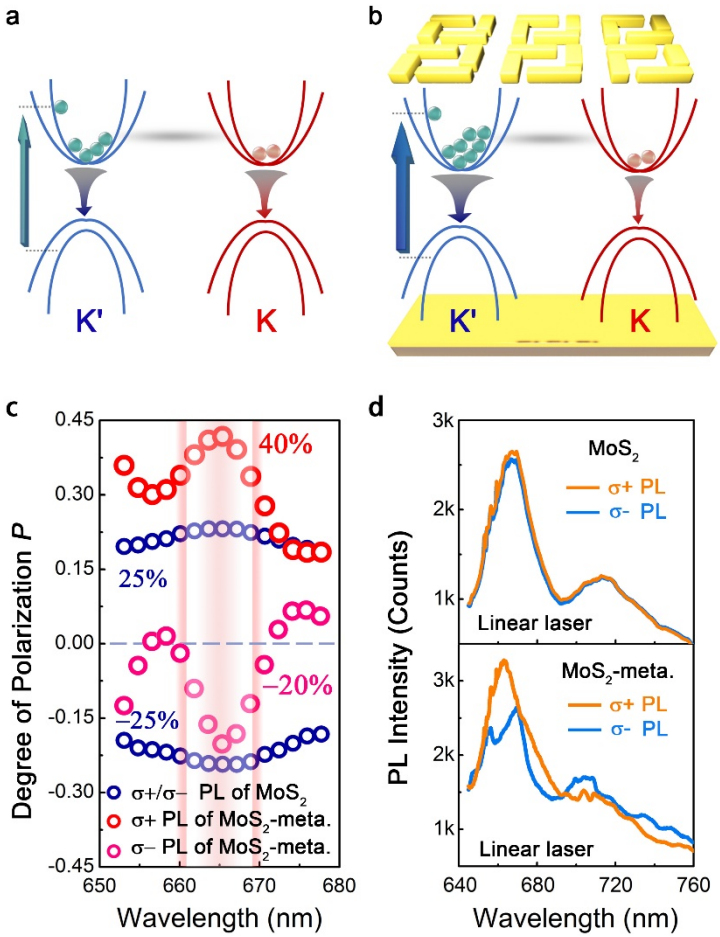

Figure 5 | Energy band and valley polarization in MoS_2-mertasurface. (a-b) Schematics of energy band of MoS_2 monolayer and MoS_2-mertasurface. (c) The DVP distribution of MoS_2 and MoS_2-metasurface. (d) Circularly polarized PL spectra of MoS_2 and MoS_2-metasurface under 633 nm linear laser excitation.

Valley polarization excited with linear polarized light. In Figure 5a-b, the tailoring mechanism of valley-polarized PL can be understood in the framework of energy band. In monolayer MoS_2, when K' valley is coupled with left-handed circularly polarized light, σ- exciton (blue balls) is generated and occupied in the lowest energy level. Some σ- exciton scatters into K valley in the channel of phonon scattering, and changes the pseudospin state to σ+ exciton (red balls) as shown in Fig. 5a. However, when monolayer MoS_2 interacts with chiral metasurface in the near-field range, the exciton absorption process is enhanced, resulting in the generation of large number of σ- exciton. The intervalley scattering process is related with temperature and excitation energy, but shows independent with local electromagnetic field. Therefore, the number of σ+ exciton scattered in the neighboring valley may not increase. In K' valley,

generated σ- exciton interacts with chiral near-field exhibiting giant optical activity, which contributes to enhanced PL intensity in the far field. In K valley, σ+ exciton emission is suppressed with the interaction of chiral field. This mechanism helps to understand the detected spectra in our experiments.

Moreover, the chiral characteristics of DVP are analyzed and compared, and the DVP near exciton energy is noted in Fig. 4a. For monolayer MoS_2, the DVP with opposite circularly polarized light excitation show nearly perfect symmetric properties, as observed as ±25%. Therefore, the absolute value of DVP in pure MoS_2 shows achiral features with opposite helicities of optical excitations. However, it shows chiral properties in MoS_2-metasurface heterostructure, which is arising from the tailoring effect of super chiral near-field. MoS_2 monolayer are endowed with alternative chirality induced by chiral metasurface, and it can be predicted that valley polarization can be observed with the excitation of linear polarized laser. The polarized PL of MoS_2 and MoS_2-metasurafce are detected using 633 nm linearly polarized light. In Fig.5d, the detected spectra of σ- and σ+ PL of pure MoS_2 show the same intensity, while remarkably, there is an obvious difference in the sample of MoS_2-metasurafce. With the induced chirality by chiral metasurface, the valley polarization of MoS_2 can be observed with simple excitation condition of linear polarized light. This experiment is a significant step toward the development of valley optoelectronics based on 2D materials.

Conclusion

In summary, we have demonstrated that valley-polarized PL of MoS_2-metasurface can be tailored in the regime of near-field interaction with circularly polarized light. The dynamics is that chiral field induced by plasmonic chiral metasurface couples with MoS_2 pseudospin valleys, which contributes to the processes of exciton absorption and emission. Compared with pure monolayer MoS_2, the DVP of MoS_2-metasurface is enhanced from 25% up to 43% with excitation of LCP light, while decreases from 25% to 20% with excitation of RCP light. Full wave simulations show that optical chirality *C* plays significant role in tailoring effect, which presents opposite signs with LCP and RCP light excitations. Monolayer MoS_2 are endowed with alternative chirality from the

plasmonic chiral metasurface, which helps to realize chiral DVP of MoS_2 at the excitation of opposite circularly polarized light. Furthermore, it has been demonstrated that valley polarization of MoS_2 can be pumped by linear polarized light, which is owing to the structural chirality of MoS_2-metasurface. Our work provides a potential platform to exploit the manipulation of valley degree of freedom in the future application of spin-valleytronic devices based on 2D materials.

Methods

Preparation of MoS_2 monolayers. MoS_2 samples were synthesized by chemical vapor deposition method (CVD). Sulfur (S) and molybdenum oxide (MoO_3) powder are the source of S and Mo, respectively. A boat with MoO_3 powder was put into a fused quartz tube located at the center of the CVD furnace. A piece of SiO_2/Si wafer was suspended on the boat. The furnace temperature was raised up to 750 °C in 15 min, and was held for 20 min, yielding MoS_2 triangle domains. During the process, 50 sccm of argon was used as the carrier gas and the growth was carried out under atmospheric pressure. Samples with spin-coated PMMA can be transferred onto prepared substrates by wetting transfer methods.

Fabrication of MoS_2-metasurface heterostructure. Au reflection layer (30 nm) and SiO_2 dielectric layer (20 nm) were deposited using e-beam evaporation system onto the prepared Si substrate chronologically. CVD-grown MoS_2 monolayers were transferred onto the SiO_2/Au/Si substrate via chemical wetting transfer technology. Another SiO_2 dielectric layer (5 nm) was then deposited to separate the MoS_2 and metasurface layer avoiding PL quenching. Finally, designed chiral metasurface was written by e-beam lithography system and then deposited with 30 nm Au film. The designed structure was drawn by nanometer pattern generation system (NPGS) and patterned by FEI Quanta scanning electron microscope (SEM). The substrate was well-prepared after lift-off process, where MoS_2 monolayers were sandwiched in SiO_2 dielectric layer, and also placed between metasurface and golden reflection layer.

Simulations and optical measurements. Simulations on electromagnetic field were performed by COMSOL and Finite-Difference Time-Domain (FDTD) solutions. And

the experimental spectra were measured by a home-built spectra system. An iHR550 Raman spectrometer from Horiba was utilized with 600 g mm^{-1} and 2400 g mm^{-1} gratings. PL spectra were measured with 600 g mm^{-1}. The objective lens is 50× magnifications. The excitation laser is 633 nm He-Ne laser, which was focused to a diffraction-limited spot about 2 μm. For the detection of valley polarization, linear polarizer (633 nm) and quarter-wave plate (633 nm) were placed after the laser irradiation. And a pair of broadband linear polarizer and quarter-wave plate (400-800 nm) were placed before the spectrometer. The cooling stage is LINKAM THMS600 system, which can control the environment temperature of sample at 87±0.2K.

Conflict of Interest: The authors declare no competing financial interest.

Acknowledgement

This work is supported by National Basic Research Program of China (973 Program, Grant No. 2015CB932403), National Science Foundation of China (Grant No. 61422501, 11674012, 11374023, and 61521004), Beijing Natural Science Foundation (Grant No. L140007), and Foundation for the Author of National Excellent Doctoral Dissertation of PR China (Grant No.201420), National Program for Support of Top-notch Young Professionals. This work is also supported by the scholarship of Graduate School of Peking University. We thank Dr. Zhigang Song for his efforts on quantum theory.

Supporting Information Available: S1. Optical properties. S2. Structural properties of metasurface. S3. Metasurface arrays. S4. PL of inversely chiral MoS_2-metasurface. S5-S6. Electromagnetic field. S7. Quantum theory. S8. Electrical dipole pairs.

References

1. Schaibley, J. R. *et al.* Valleytronics in 2D materials. *Nat. Rev. Mater.* **1**, 16055 (2016).
2. Mak, K. F., McGill, K. L., Park, J. & McEuen, P. L. Valleytronics: The valley Hall effect in MoS_2 transistors. *Science* **344**, 1489-1492 (2014).

3. Eginligil, M. *et al.* Dichroic spin-valley photocurrent in monolayer molybdenum disulphide. *Nat. Commun.* **6**, 7636 (2015).
4. Xu, X., Yao, W., Xiao, D. & Heinz, T. F. Spin and pseudospins in layered transition metal dichalcogenides. *Nat. Phys.* **10**, 343-350 (2014).
5. Hsu, W. T. *et al.* Optically initialized robust valley-polarized holes in monolayer WSe_2. *Nat. Commun.* **6**, 8963 (2015).
6. Gong, Z. *et al.* Magnetoelectric effects and valley-controlled spin quantum gates in transition metal dichalcogenide bilayers. *Nat. Commun.* **4**, 2053 (2013).
7. Xiao, D., Liu, G. B., Feng, W., Xu, X. & Yao, W. Coupled spin and valley physics in monolayers of MoS_2 and other group-VI dichalcogenides. *Phys. Rev. Lett.* **108**, 196802 (2012).
8. Mak, K. F., He, K., Shan, J. & Heinz, T. F. Control of valley polarization in monolayer MoS_2 by optical helicity. *Nat. Nanotechnol.* **7**, 494-498 (2012).
9. Cao, T. *et al.* Valley-selective circular dichroism of monolayer molybdenum disulphide. *Nat. Commun.* **3**, 887 (2012).
10. Wang, X. *et al.* Chemical vapor deposition growth of crystalline monolayer $MoSe_2$. *ACS Nano* **8**, 5125-5131 (2014).
11. He, K. *et al.* Tightly bound excitons in monolayer WSe_2. *Phys. Rev. Lett.* **113**, 026803 (2014).
12. Yu, T. & Wu, M. W. Valley depolarization due to intervalley and intravalley electron-hole exchange interactions in monolayer MoS_2. *Phys. Rev. B* **89**, (2014).
13. Onga, M., Zhang, Y., Ideue, T. & Iwasa, Y. Exciton Hall effect in monolayer MoS_2. *Nat. Mater.* **16**, 1193-1197 (2017).
14. Ye, Y. *et al.* Electrical generation and control of the valley carriers in a monolayer transition metal dichalcogenide. *Nat. Nanotechnol.* **11**, 598-602 (2016).
15. Yang, W. *et al.* Electrically tunable valley-light emitting diode (vLED) based on CVD-grown monolayer WS_2. *Nano Lett.* **16**, 1560-1567 (2016).

16. Dufferwiel, S. *et al.* Valley-addressable polaritons in atomically thin semiconductors. *Nat. Photon.* **11**, 497-501 (2017).
17. Sun, Z. *et al.* Optical control of room-temperature valley polaritons. *Nat. Photon.* **11**, 491-496 (2017).
18. Zhang, X. X. *et al.* Magnetic brightening and control of dark excitons in monolayer WSe_2. *Nat. Nanotechnol.* **12**, 883-888 (2017).
19. S. Gong, Alpeggiani, F., Sciacca, B., Garnett, E. C. & Kuipers, L. Nanoscale chiral valley-photon interface through optical spin-orbit coupling. *arXiv:1709.00762* (2017).
20. Cerjan, B., Yang, X., Nordlander, P. & Halas, N. J. Asymmetric Aluminum Antennas for Self-Calibrating Surface-Enhanced Infrared Absorption Spectroscopy. *ACS Photon.* **3**, 354-360 (2016).
21. Yin, X. *et al.* Active Chiral Plasmonics. *Nano Lett.* **15**, 4255-4260 (2015).
22. Duan, X., Kamin, S., Sterl, F., Giessen, H. & Liu, N. Hydrogen-Regulated Chiral Nanoplasmonics. *Nano Lett.* **16**, 1462-1466 (2016).
23. Hentschel, M., Schäferling, M., Duan, X., Giessen, H. & Liu, N. Chiral plasmonics. *Sci. Adv.* **3**, e1602735 (2017).
24. Tang, Y. & Cohen, A. E. Enhanced enantioselectivity in excitation of chiral molecules by superchiral light. *Science* **332**, 333-336 (2011).
25. Hendry, E. *et al.* Ultrasensitive detection and characterization of biomolecules using superchiral fields. *Nat. Nanotechnol.* **5**, 783-787 (2010).
26. Liu, W. *et al.* Strong Exciton-Plasmon Coupling in MoS_2 Coupled with Plasmonic Lattice. *Nano Lett.* **16**, 1262-1269 (2016).
27. Tang, Y. & Cohen, A. E. Optical chirality and its interaction with matter. *Phys. Rev. Lett.* **104**, 163901 (2010).
28. Schäferling, M., Dregely, D., Hentschel, M. & Giessen, H. Tailoring Enhanced Optical Chirality: Design Principles for Chiral Plasmonic Nanostructures. *Phys. Rev. X* **2**, 031010 (2012).

29. Nesterov, M. L., Yin, X., Schäferling, M., Giessen, H. & Weiss, T. The Role of Plasmon-Generated Near Fields for Enhanced Circular Dichroism Spectroscopy. *ACS Photon.* **3**, 578-583 (2016).

30. Ren, Q. *et al.* Spin-resolved Purcell effect in a quantum dot microcavity system. *Nano Lett.* **12**, 3455-3459 (2012).

31. Maksimov, A. A. *et al.* Circularly polarized light emission from chiral spatially-structured planar semiconductor microcavities. *Phys. Rev. B* **89**, 045316 (2014).

32. Lobanov, S. V. *et al.* Controlling circular polarization of light emitted by quantum dots using chiral photonic crystal slabs. *Phys. Rev. B* **92**, 205309 (2015).

33. Li, Z. *et al.* Tailoring MoS2 Exciton-Plasmon Interaction by Optical Spin-Orbit Coupling. *ACS Nano* **11**, 1165-1171 (2017).

34. Li, Z. *et al.* Graphene Quantum Dots Doping of MoS_2 Monolayers. *Adv. Mater.* **27**, 5235-5240 (2015).

35. Zeng, H., Dai, J., Yao, W., Xiao, D. & Cui, X. Valley polarization in MoS_2 monolayers by optical pumping. *Nat. Nanotechnol.* **7**, 490-493 (2012).